Progress In Electromagnetics Research B, Vol. 28, 75–94, 2011

MIMO RADAR ARRAY FOR TERMITE DETECTION AND IMAGING

N. W. D. Le Marshall

University of NSW@ADFA
Australia

A. Z. Tirkel

Scientific Technology
Australia

Abstract—In this paper, we describe the design of a hybrid 24 GHz RADAR array for termite detection and imaging. The array uses MIMO techniques to provide transmit beam steering and null steering in conjunction with the Matrix Enhanced Matrix Pencil (MEMP), which provides direction of arrival processing. We describe the selection of our MIMO orthogonal codes and test their suitability. Simulated results are shown for our array design and MIMO processing in a range of applications MIMO enables us to produce flexible nulling and beam steering for our transmitter array as well as reducing multipath reflections and narrowband interference. MIMO processing also produces large time savings, enabling longer, more accurate acquisitions which can increase SNR. Transmitter beamforming, produces an SNR improvement of 18.2 dB and can be used to reject clutter by up to 20 dB. Flexible nulling can reject interferers still further.

1. INTRODUCTION

The presence of termites is difficult to detect due to their subterranean habitat, yet they cause billions of dollars in structural and cosmetic damage every year [1]. Currently, the only way to reliably detect termites without physical damage to the structure under investigation is to use a hand held 24 GHz RADAR device developed by our group and commercialized by Termatrac® [2]. Other methods of

Received 28 October 2010, Accepted 4 January 2011, Scheduled 26 January 2011
Corresponding author: Nick W. D. Le Marshall (nick.lemarshall@student.adfa.edu.au).

non-invasively detecting termites such as vibration sensing and gas detection have proven less effective than movement detection via RADAR.

Termatrac® uses a single fixed RADAR beam to detect movement of insects inside structures. This is difficult due to the very low Signal to Noise Ratio (SNR) and the returns from clutter which are more than 60 dB greater than the signals returned from the insects (which have a very low scattering cross-section). We separate the changing termite signals from stationary background clutter via a 0.1 to 10 Hz band pass filter, a technique which has been proven over years of field experience to pass the relevant signals. Incidental movement of the instrument results in relative movement of the background clutter in the RADAR signal and reduces the effectiveness of this filtering. From the Nyquist criterion, the minimum sample rate (or frame rate for an imaging instrument) is 20 Hz in order to capture termite motion within the filter bandwidth. Field testing has shown that the minimum dwell time is between 1 s and 10 s.

A device which could scan a large area at once and provide high resolution imaging would be a major improvement. Such a device is the subject of this paper. Scanning a large area is achieved by deploying a Direction of Arrival (DOA) algorithm in the far field. High resolution imaging is achieved by near field beamforming. The resolution of the near field imaging algorithm should permit the tracking of single termites and cover an area of at least 0.25 square meters at a distance of 500 mm.

Since termites are small, they scatter weakly, so that high resolution can only be achieved at short ranges where SNR is acceptable. Short range signals result in significant wave front curvature, a result known as the near field effect [3]. Wide area coverage requires long range, resulting in low SNR. These competing requirements for wide area coverage and high resolution are unlikely to be achieved with a single array. As a result, our solution involves a hybrid array, which has a single transmit array and dual receive arrays. It uses a compact 5×5 receive sub-array to cover a wide area, from a long range (500 mm or greater), providing direction of arrival (DOA) information about any insect activity, using a Matrix Pencil DOA algorithm. At the array periphery, a receive array with random geometry provides 3D imaging at short ranges (100 mm and less) using beam-forming and focusing algorithms. The transmit array consists of a multi-ring uniform circular array. Circular array geometry was selected for the transmitter to provide uniform illumination in azimuth and low side-lobes. The sparse random array geometry is preferred for our beam-forming network. Such an array has fewer elements than

a regular array of comparable size, but suffers minimal reduction in resolution. The random array sidelobe levels can be bounded by an optimization technique, and the larger inter-element spacing reduces mutual coupling, and permits easier placement of support circuitry and feed networks. The Array Geometry is shown in Figure 1.

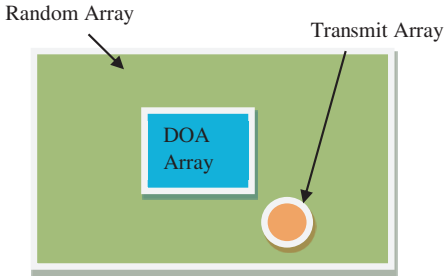

Figure 1. Array geometry — transmit array is a concentric circular array supporting MIMO usage. Central DOA array has elements arranged in regular rectangular grid. Random receive array supports imaging at close range.

This paper is mainly concerned with the implementation of the far field direction of arrival determination. Specifically, we describe a new application of Multiple In-Multiple Out (MIMO) techniques to enhance the accuracy of the results achieved using a Direction of Arrival (DOA) technique. The DOA accuracy is enhanced due to an increase in the SNR and reduction in clutter and influence of interfering targets. The performance and implementation of the random array and our MIMO beamforming and focusing algorithm, which is used for imaging at short range, is discussed in a separate paper [4]. Additional discussion of the capabilities of our transmit beam-former can be found in [5].

At long range (greater than 500 mm) we obtain DOA by the Matrix Enhanced Matrix Pencil (MEMP) algorithm [6]. The MEMP algorithm was selected because it functions with only a single snapshot, provides native processing of coherent signals and superresolution accuracy compared with spectral estimation and ESPRIT [7] and MUSIC [8], which by default require incoherent signals. Although certain techniques can allow MUSIC and ESPRIT to operate with coherent signals, such as forward-backward averaging [9], this reduces the number of effective array elements, thus lowering the resolution, SNR and maximum number of targets detected. Such averaging algorithms also require tens of snapshots spaced in time. In order to enhance the SNR during the MIMO correlation, we already perform averaging of received signals over many samples. As a result, multiple

snapshots are costly, and a DOA algorithm which requires only a single snapshot is desirable. The authors have discussed the rationale for selection of the MEMP algorithm previously [4, 5, 10, 11].

MEMP performance is dependent on received SNR [6]. Covering wide areas, remaining within allowable maximum transmit power limits and satisfying required MEMP signal levels simultaneously is challenging. One method of enhancing the power delivered to a target is by using a directional transmitter, which scans the area of interest. Traditionally transmitter directivity has been achieved by steering the transmit beam either mechanically or electronically via transmit array phasing. Forming individual transmit beams sequentially greatly increases acquisition times. Hardware that produces arbitrary signals at each of its elements in order to generate the desired beam patterns is difficult to construct, and the beam control, and hence the results are inaccurate. By contrast, processing the digitized signals from the receiver elements is more precise, and can be performed in parallel, in a Field Programmable Gate Array (FPGA), decoupled in time from signal reception. Receiver array phasing is not compatible with the MEMP [10]. Therefore, Multiple Input Multiple Output (MIMO) processing, which allows transmitter beamforming after digitization at the receiver, is an attractive solution.

In our implementation, the transmitter elements are fed signals which are modulated by a set of orthogonal codes. At each receiver element, the signals from transmitter elements are able to be processed separately and in parallel, allowing transmitter "virtual" beamforming to be implemented before the DOA processing. Because only a single acquisition is required to compute all possible beams and virtual array patterns, the acquisition time is massively reduced. The time that has been saved can be invested into averaging of received data for noise reduction or a slower but lower noise acquisition system. Ideally, using 33 elements for transmit beamforming via MIMO we would also expect an increase in the SNR of $10 \log_{10} 33 = 15.185$ dB, plus an additional 3 dB gain from the element pattern for a total gain of 18.2 dB as compared to a single isotropic antenna using transmit power equal to the sum of all the individual MIMO transmit antennas (i.e., 33 times the power of a single MIMO antenna). In addition, the transmit beamforming, when focussed on a target will reject clutter by up to 20 dB (see Section 6 and 8). The transmit beam-forming can also be used to produce flexible nulling which can reject clutter by a larger amount.

In this paper, the terms focusing and beam-forming are used interchangeably. We regard the focusing technique as a subset of general beam-forming technique, where a focused array is one in which

the transmitted (or received) signals are phase aligned at a point in 3D space.

This paper is organized as follows: Section 2 describes the physical structure of our array and support hardware. Section 3 describes our application of the matrix pencil and our modifications to it. Section 4 describes our implementation of MIMO processing for the array. Section 5 describes the orthogonal codes used in our MIMO implementation. Section 6 describes the typical array patterns generated by our transmitter. Section 7 describes our methods of optimizing array patterns for the transmitter. Section 8 shows simulated results for beamforming and null steering of the transmitter. Section 9 describes methods of using our MIMO array to enhance the performance of the MEMP algorithm.

2. HARDWARE DESCRIPTION

Our array consists of 89 receive elements and 33 transmit elements (Figure 2 is an early prototype). The receive elements are distributed across the array as two sub-arrays with distinct geometries, designed for long and short range usage. The central area of the receive array consists of a densely packed regular square array for long range direction of arrival sensing, exhibiting a short far-field range of 200 mm and a geometry compatible with the matrix pencil algorithm. The sparse, random, peripheral receiver sub-array can also be seen. In addition to the receive elements, there is a transmitter array consisting of 33 elements arranged in 3 concentric circular rings. Figure 2 below shows a previous iteration of our array that has been laid out for fabrication. The version shown has very similar geometry but contains only a single ring of transmit elements.

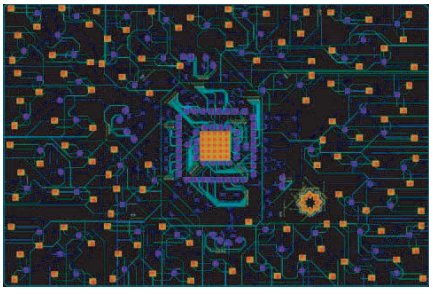

Figure 2. Hybrid array. Three distinct regions can be observed; a central dense receive array for far field use, a peripheral random receive array, and a small transmit array at lower right of the figure.

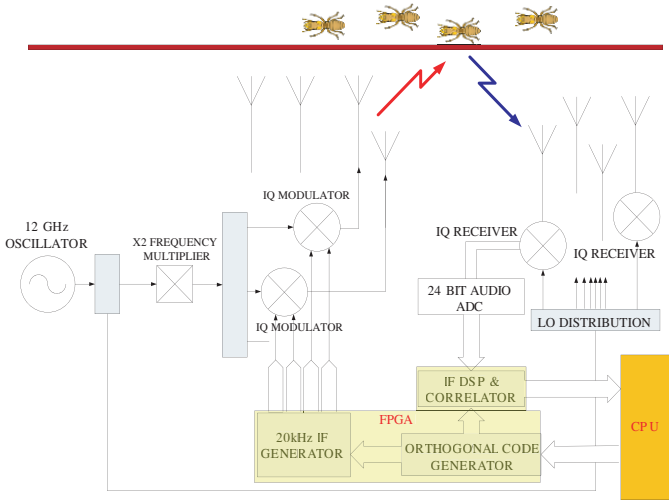

Figure 3. MIMO array block diagram-frequency up/down conversion performed via quadrature mixer with Tx array on left and Rx array on right. IF digitization via high resolution ADC with samples delivered to FPGA for initial processing. FPGA provides Rx & Tx control and MIMO processing. The CPU provides system control and user feedback.

The number of transmit and receive elements was selected to meet our performance goals for transmitter beam-forming and resolution, and avoiding aliasing. The aliases are false targets which are generated due to insufficient sampling (i.e., elements) in the spatial domain. Figure 3, depicts a transmitter element and a receiver element signal processing, including internal functional blocks implemented in a FPGA. The Field Programmable Gate Array (FPGA) provides the digital signal processing (DSP) needed to implement the direction of arrival and high resolution imaging capabilities.

The scheme uses quadrature upconversion in the transmitter and downconversion in the receiver. The baseband signal utilizes a 20 KHz offset or intermediate frequency (IF), which is added and removed digitally. The 20 KHz IF enables the use of high resolution (24 bit) audio Analog to Digital Converters (ADCs) and avoids aliasing of the down-converted signals. The array uses MIMO techniques as detailed in Section 4, with the FPGA used for generating the reference codes, and correlating the received signals. The FPGA is also employed for beam-forming and MEMP calculations. Recent advances in FPGA and DSP hardware have enabled the use of these devices in cost-effective, battery powered applications [12].

3. MATRIX ENHANCED MATRIX PENCIL (MEMP)

The MEMP is our method of choice for direction of arrival estimation primarily because it requires only a single snapshot of the data and functions effectively with correlated signals [6]. Our signals are correlated, due to the short time of flight of the signals (a few nanoseconds). Signals received by a regular rectangular array with element spacing (Δ_x, Δ_y) can be modeled using Equation (1) [13]:

$$x(m:n) = \sum_{p=1}^{p} A_p \exp(j\gamma_p + 2\pi m\Delta_x \sin\theta_p \cos\varphi_p + j2\pi n\Delta_y \sin\theta_p \sin\varphi_p) \tag{1}$$

where p is an index of received signals from targets labeled from 1 to $P, j = \sqrt{-1}$, A_p is the amplitude of the pth target, γ_p is the phase, φ_p is the elevation and θ_p is azimuth. The signal sample values are assembled into a matrix with enhanced rank condition using a partition and stack process [13]. A Singular Value Decomposition (SVD) is used to estimate the number of targets present. This establishes the signal and noise subspaces within the data matrix. Three sets of eigenvalues are determined by matrix inversion, and are used to estimate the azimuths and elevations of all the targets in the signal subspace. For elevation and azimuth we need a pair of eigenvalues (or poles) which when multiplied are equal to an eigenvalue from the third set. The correct estimation of the values relies on correct pairing, and we perform a search to select the best triplets of eigenvalues (one from each set). Amplitude and phase information can also be estimated by this process [13].

The MEMP requires a uniform rectangular array to function. Any deviation from ideal array geometry or element response causes degradation in the MEMP accuracy. These deviations can result from factors such as limitations in physical element placement, phase and amplitude balance of each receiver element, manufacturing tolerances, and mutual coupling.

In order to compensate for these non-ideal geometries, we introduce a matrix based array transformation. The transformation matrix, T, is calculated as the least mean squared solution to:

$$T = \arg\min_T ||TA_R(\phi_i, \theta_i) - A_V(\phi_i, \theta_i)||_F^2 \tag{2}$$

where A_R and A_V are the array manifolds from a set of angles generated from simulation or calibration data for the real and virtual array respectively [14, 15].

This transformation matrix is effective at compensating for the issues outlined above, but any single transformation matrix is only

accurate over a restricted range of target angles. This range of angles is known as the array transformation sector. In order for the transformed data to be accurate, the input to the transformation matrix must be spatially filtered to exclude signals from outside the sector (a range of angles in azimuth and elevation) for which the transformation has been computed. The authors have previously used signal cancellation to remove out-of-sector signals [4], but in this paper we propose to use MIMO transmitter beam forming to perform a similar function, but with the additional benefits of spread spectrum processing, or to complement the cancellation method by providing better suppression of out of sector targets.

4. MIMO IMPLEMENTATION

Since MEMP and most other DOA algorithms rely on analysis of the phase advance across the receiver array to determine the direction of arrival of incoming signals [6], phased array receiver techniques are not suitable, as they alter the phase information in the received signals. Transmitter beamforming by amplitude and phase control is permissible, but hardware phase and amplitude modulation of a large number of transmitter elements is complex, difficult to achieve, inaccurate, and only one beam can be formed at a time. Another approach is to use a MIMO technique [16] whereby each transmitter element broadcasts a known unique code, with all codes being mutually orthogonal. At each receiver element, the received signal is correlated with each of the orthogonal codes, to determine the magnitude and phase of the signal received from a particular transmitter element [16]. The results of these correlations are multiplied by complex weights and added to form an arbitrary "virtual" transmitter beam. This multiplication is performed digitally, after the analog to digital conversion of the receiver signals. In this scheme, the only transmitter control is biphase modulation. This is less complex than conventional transmitter beamforming, which requires arbitrary phase and magnitude control of each transmitter element. A basic block diagram of the software processing is shown in Figure 4.

With MIMO, the beamforming processing can occur independently (and in parallel) with the reception of transmitted signals. This allows the computation of all possible beams from a single acquisition, greatly reducing the time requirements and exploiting the parallel nature of current DSP systems. By comparison, a system without MIMO must generate transmit beams via complex modulation of the RF signals, one beam at a time, allowing time for signal reception after each modulation change.

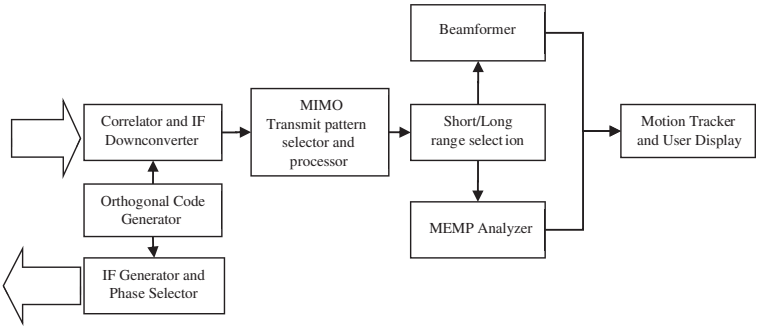

Figure 4. Basic block diagram of software processing.

The results generated by multiple parallel runs of the MIMO system, when combined into a single image exhibit less "motion blur" of the target. The greater speed of the MIMO system which enables us to either use averaging of the samples and hence achieve greater SNR or select a slower but higher accuracy acquisition system (e.g., a higher accuracy analog to digital converter).

Our MIMO system, which uses codes with good auto-correlation properties (see Section 5), is a spread spectrum system, and hence enables an increase in the SNR due to processing gain where there is narrowband interference.

5. MIMO CODE DESIGN

The primary requirement of the code set is orthogonality in order to minimize interference between signals. A secondary requirement is good autocorrelation. We also desire spectral equivalence, so that any distortions or interference affect all codes equally. The code should also have a simple alphabet, which eases implementation. By definition, the rows or columns of any Hadamard Matrix satisfy the primary requirement. Our design has 33 transmitter patches and hence requires 33 orthogonal codes. Our preferred set of codes (which satisfies all the requirements) is obtained from the cyclic shifts of a pseudonoise twin-prime sequence of length 35 [17]. This results in a 36×36 Hadamard Matrix (after the addition of a row and column of 1's, required for zero cross-correlation and set completion respectively). Any 33 of the 35 non-constant codes are suitable for our application. An example of such a code is:

$$[1, 1, -1, 1, 1, 1, -1, -1, -1, 1, 1, 1, 1, 1, -1, 1, 1, 1, -1,$$
$$-1, 1, -1, -1, -1, -1, 1, -1, 1, -1, 1, 1, -1, -1, 1, -1, -1]$$

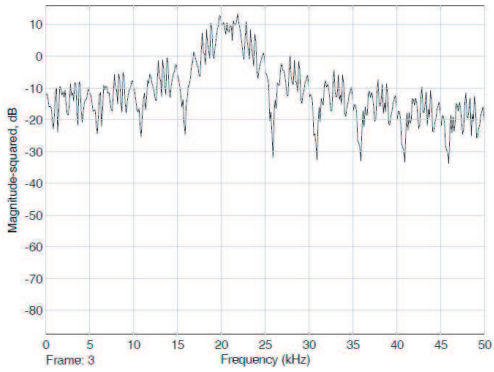

Figure 5. Power spectral density of IF signal before correlation.

The spectral properties of such a code, for the chosen IF frequency, are shown in Figure 5. The spectra for the other 32 orthogonal codes are similar. The IF frequency is chosen to be 20 kHz, which is high enough to avoid $1/f$ noise problems (the ubiquitous noise exhibited by many physical systems resulting in the spectral density having the form $1/f^{\propto}$, where f is the frequency and $\propto$ is a constant [18, 19]), and low enough to be adequately sampled by a commercial audio ADC. The chip rate is 5 kHz. The codes are transmitted using a Binary Phase Shift Keying (BPSK) modulation. Our transmitter is based on a Direct Digital Synthesis (DDS) device and hence gain and phase is adjustable at the transmitter required in order to allow for optimization of the transmit pattern and mutual coupling reduction strategies [20]. Optionally, as we have a MIMO device, we can perform the gain and phase adjustment at the receiver after reception.

It should be noted that our application does not require low off-peak autocorrelation from our codes, because the maximum round trip signal delay, and delay spread is less than 10 ns, compared with a chip period of 0.2 ms. Fundamentally our system is synchronous, hence correlation only needs be considered with a zero delay. Our system has very low cross-correlation.

6. MIMO ARRAY PATTERN

Our transmitter is used in two modes. In the case of the 3D imaging mode, MIMO processing is used to focus the transmit pattern onto a volumetric pixel (voxel) to maximize the return from this location. In the case of the direction of arrival processing, the array pattern is used

to form beams and nulls in particular directions to reduce returns from unwanted targets and increase illumination of wanted targets.

A complete simulation of our proposed MIMO transceiver has been constructed. Figure 6 and Figure 7 show the performance of the transmitter array focused on a point in 3D space. The magnitude of the array patterns are shown in dB scale on a polar axis. These array patterns can be used both to improve the resolving power of the array when imaging, and to increase rejection of out of sector signals when used with the MEMP.

Figure 6 shows a cross section of the transmit pattern at 125 mm range. The beam can clearly be seen with over 20 dB attenuation for all but the first sidelobes. The pattern shows a significant backlobe, around 10 dB higher than the sidelobes (around the same power as the first sidelobes), but for the beam-formed array this is less of an issue because the receiver beamforming can be used to reject it.

For the MEMP array, receiver spatial filtering is not possible [10, 11], so the targets illuminated by this backlobe have to be rejected by other means The backlobe still maintains more than 10 dB of rejection, and hence is more desirable than an isotropic transmitter pattern.

Figure 7 shows a cross section along the azimuth plane. We can see here that the transmit array adds at least 5 dB of rejection over the range of interest Note that these patterns show the near field of the array.

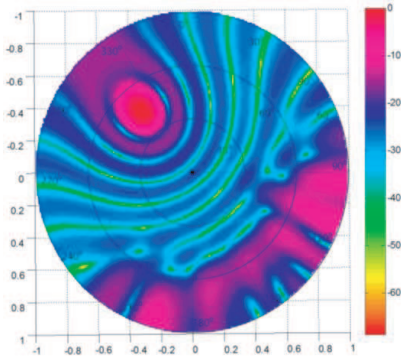

Figure 6. 3D transmit pattern slice at 125 mm range. Transmitter is focused at 45 degrees elevation and 320 degrees azimuth and 125 mm range. Units in dB.

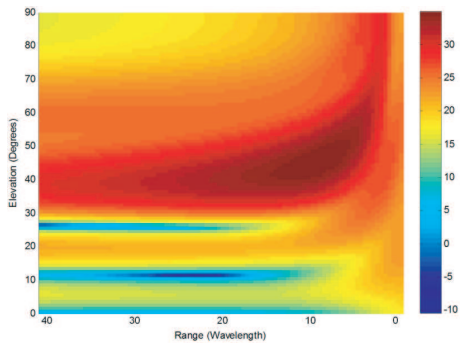

Figure 7. 3D transmit pattern slice at 50 degrees azimuth. Transmitter is focused at 45 degrees elevation and 50 degrees azimuth and 125 mm (10 wavelengths) range. Units in dB.

7. TRANSMITTER PATTERN OPTIMIZATION AND NULL STEERING

As discussed in Section 2, the MEMP requires an array transformation to compensate for any non-ideal properties of the receive array, such as mutual coupling, or lack of a perfect rectangular geometry, or non-uniform antenna or receiver response. Since the transformation is accurate over a sector only, out of sector targets must be filtered. Some of this can be achieved by transmit pattern beam forming. In addition, the transmit pattern can be altered to include nulls at specific locations. This allows us to exclude specific regions, in order to enhance the dynamic range, or to confirm the location of features by their absence when the nulls are present, or simply to null out an unwanted target. The selection of filter weights can be stated as an optimisation problem with the following constraints:

$$\begin{aligned}&\text{Minimize max (abs } (A_s W))\\&\text{Subject to:}\\&A_{tar} W = 1\\&A_{null} W = 0\end{aligned}$$

where W are the array weights, A_{tar} is an array steering vector in the desired beam direction, A_{null} is a set of array steering vectors in the direction of the nulls, and A_s is a set of array steering vectors that cover directions not in the direction of the beam nor in the direction of the nulls.

This problem is suitable for convex optimization via disciplined convex programming [21], which enables us to transform a simple set of rules defining our desired array pattern for use by a convex optimization algorithm. We used the CVX analysis package [22] and the SDPT3 solver [23] to generate optimum array patterns for our array. Convex optimization was chosen as a valid and rapid method of finding an optimum set of weights producing either a desired beam, desired nulls or both in the transmit pattern. Other examples of convex optimization of array patterns can be seen in the literature [24]. Results from several common array geometries including single ring circular, rectangular and multi-ring circular arrays were compared, and the multi-ring circular (with the appropriate number of elements) was found to be the most consistent in side-lobe suppression and number of nulls that could be formed [5]. The CVX analysis package took between 1 and 10 minutes to solve the optimization problem on a 2 GHz dual core processor with MATLAB 2010A.

It should be noted that this process and the following results are for far field patterns (i.e., with planar wavefronts) whereas the previous

results in Section 6 are for near field patterns where the wavefronts are modeled as spherical.

8. BEAMFORMING AND NULL STEERING RESULTS

Convex optimization was performed on the array pattern for a 3 ring circular array with array elements per ring of 5, 11 and 17 from inner to outer ring. Element spacing was 0.5 wavelengths along the circumference of the outer ring. This is based on the ideal spacing for a Chebyshev spatial filter using a uniform concentric circular array [25], which achieves the design beamwidth/null width with equal amplitude ripple outside the beam or null. Simulation results are shown below (Figure 8 through Figure 11) for a variety of array pattern constraints. These array patterns are far field simulations.

Figure 8 demonstrates the beamforming performance of our array using convex optimization with the resulting beam at least 15 dB above the sidelobes. In Figure 9, we can see an arbitrary null being formed from four point nulls, in this case an 'X' shaped null is formed. These arbitrary nulls can be used to select "null out" features which interfere with our scanning. They can also be used to mask targets that have been analyzed in a previous scan.

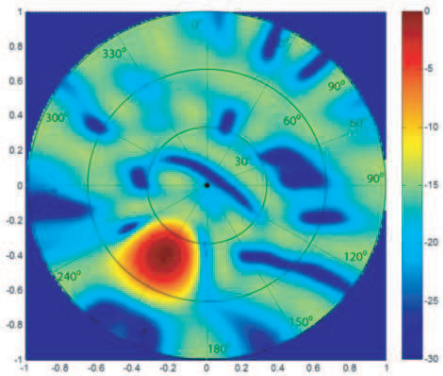

Figure 8. 2D transmit pattern projected onto unit circle. Power in dB. Negative range has been truncated to enhance beam visibility. For this pattern we have optimized the array pattern to provide a scanning beam at 210 degrees azimuth and 45 degrees elevation.

Figure 10 shows an azimuthal null at 35 degrees. Figure 11 shows an elevation null formed at 20 degrees of elevation, in combination with a main beam at 210 degrees of elevation. Placement of a main beam is accurate to within a few degrees, although the beam shape can be

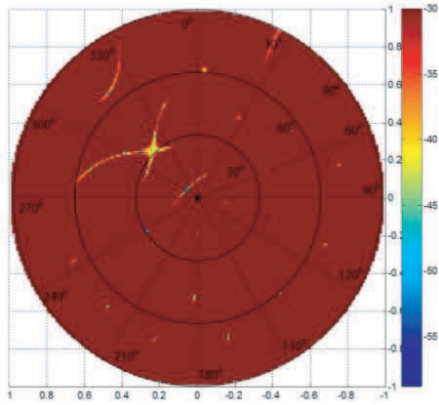

Figure 9. 2D transmit pattern projected onto unit circle. The angular coordinate is azimuth in degrees, and the radial coordinate is elevation in degrees. Power in dB relative to maximum beam power. Maximum power has been truncated in the plot to highlight position of nulls. The nulls were constrained to 4 points (310 : 34, 310 : 29, 320 : 34, 320 : 29 azimuth: elevation degrees) in order to produce an 'X' shape. The main beam is not visible here due to truncation of displayed power, but is similar to that shown in Figure 8.

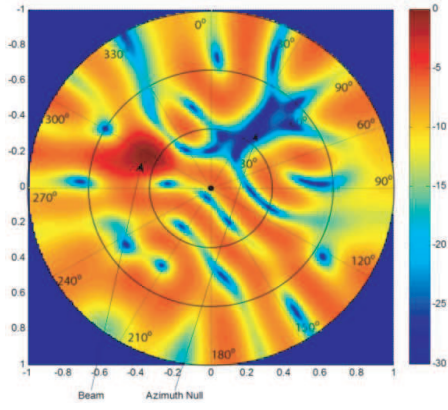

Figure 10. 2D transmit pattern projected onto unit circle. Power in dB relative to maximum beam power. This shows an azimuth null at 35 degrees extending from 15 to 65 degrees in elevation as well as the main beam at 45 degrees elevation and 300 degrees azimuth. Azimuth Null and beam direction can be seen.

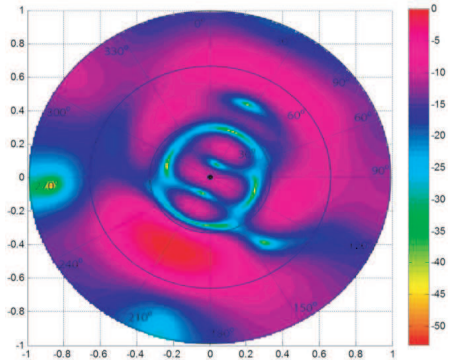

Figure 11. 2D transmit pattern projected onto unit circle. Power in dB relative to maximum beam power. Shows elevation null at 20° as well as beam at 210 degrees elevation and azimuth.

distorted by the presence of nearby nulls, as in Figure 10 and Figure 11; however, we can determine how closely the array pattern matches our constraints as we form it. This allows us to reject any pattern that has unacceptable distortions or unintended nulls in problematic positions. In addition, multiple array patterns can be combined to form complex patterns of nulls. We have found that the convex optimization performs best when given a limited number of constraints to optimize for, and hence this would enable us to accurately produce more complex patterns.

9. MEMP WITH TRANSMIT BEAMFORMING AND NULL STEERING

Combining the null steering via convex optimization with the MEMP, we can evaluate whether the combination performs as designed. Two situations are analyzed.

In the first situation, we attempt spatial filtering of targets outside the array transformation sector via transmitter beam forming. To achieve this, a reduction in target amplitude of 15 dB was deemed sufficient. The transmitter array pattern used can be seen in Figure 8 above. This array pattern contains a single beam with no constrained nulls.

We simulated 2 targets received by the MEMP array, with one target in sector and the other target outside the sector. Targets that are outside the target sector undergo an inaccurate array transformation, with distortion of the received array pattern for this

target and consequent inaccuracies in reported target positions. In some positions, this out of sector target was able to cause the MEMP to fail to resolve any targets. We then applied the transmit array beam-forming to the simulation, suppressing the out of sector targets. The results can be seen in Figure 12 and Figure 13 below.

In the figures above, we can see that Tx beam-forming has effectively suppressed the out of sector far field target (visible at 0 degrees azimuth in Figure 12). This far field target is no longer resolved by the MEMP, and is not visible in Figure 13. In addition, the positions of the 2 near field targets are estimated more accurately.

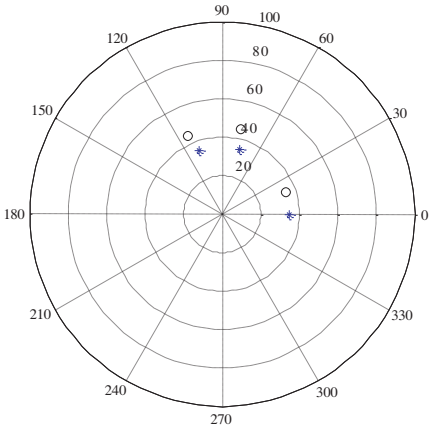

Figure 12. Two in sector near field and one out of sector long range target. Blue star indicates actual position of target. Circles indicate estimated position of target. All targets at 35 degrees elevation. Near field targets are at 75 and 114 degrees azimuth. Far field target at 0 degrees azimuth. All targets have equal amplitude. Near field targets are at range 10 wavelengths. Far field targets are at 50 wavelengths.

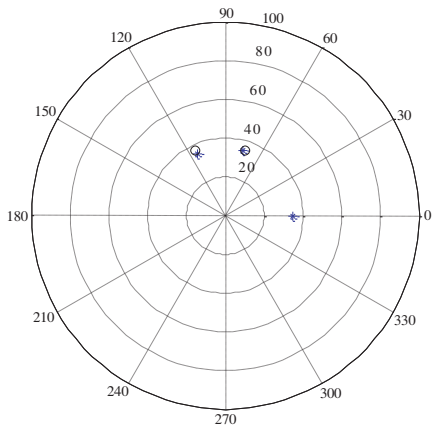

Figure 13. Two in sector near field and one out of sector long range target. Blue star indicates actual position of target. Circles indicate detected position of target. All targets at 35 degrees elevation. Near field targets are at 75 and 114 degrees azimuth. Far field target at 0 degrees azimuth. All targets have equal amplitude, but far field target is attenuated approximately 15 dB using Tx beamforming and is not resolved by matrix pencil. Near field targets are at range 10 wavelengths. Far field targets are at 50 wavelengths.

In the second case, we examine the null steering performance, where both the targets of interest and the signal we wish to attenuate (by superimposing a null) are in the same sector. This method may be used to reduce the number of targets seen by the MEMP algorithm, avoiding situations where the number of targets present is more than the MEMP is capable of estimating. In a rectangular array that is M by N elements, the standard MEMP algorithm supports a maximum number of targets that is equal to either $M-1$ or $N-1$, whichever is less [6].

A split beam is a useful array pattern in our application as it would enable the detection of termites as they cross the null between the two beams. Although any pattern with a main beam and/or and constrained nulls could be used, we have used a pattern with a split beam for this analysis. This occurs when the null is constrained to be inside the beam formed by the transmit array. The results of this constraint can be seen in Figure 14.

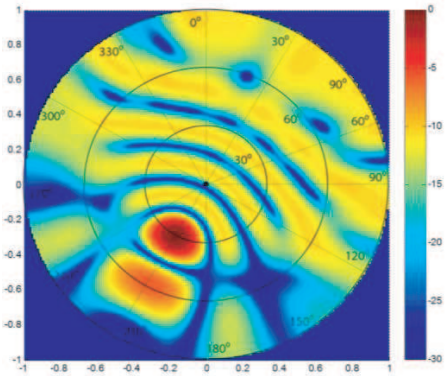

Figure 14. Split beam array pattern.

This array pattern can be used where we wish to illuminate a sector while "nulling out" some targets within this sector. A simulation was performed using this array pattern to remove a target from the sector of interest while preserving a second target. Results were similar to those shown in Figure 12 and Figure 13 above, with the target at the null location unresolved by the MEMP algorithm.

Both of these simulations show the utility of the convex optimized array pattern generation. We have determined that the patterns displayed above correctly perform the actions that they are designed for, with the targets positioned at the nulls being reduced in magnitude by more than 50 dB, resulting in them being effectively excluded from the matrix pencil analysis. It should be noted that the true depth

of nulls is not shown in any of the figures to avoid scaling issues. Rather, the minimum power has been truncated to a fixed value which highlights relevant features.

It should be noted, that our simulations do not take into account the distortion of the array pattern that will be induced when materials are introduced into the arrays environment (as would occur when the termites were concealed behind a wall). Although our high pass filter will reliably remove these non-moving objects from the data, the change in path length may distort the images and array patterns that we calculate. The authors are currently tackling the issue of reducing the distortion caused by the introduction of RADAR translucent objects into the field of view.

The authors have developed a method of removing or reducing the effective magnitude of out of sector targets via cancellation [4]. The beam-forming and nulling available via MIMO techniques can be combined with the cancellation algorithm, potentially suppressing out of sector targets by a total of 40 dB. Alternately, the MIMO method can replace the cancellation method, providing similar results combined and adding the other benefits of MIMO processing.

10. CONCLUSIONS

We present a hybrid array for detecting and imaging termite activity behind a wall, floor, or ceiling. Adding MIMO can reduce interference, improve the speed of acquisitions, and improve the discrimination of targets, as shown in our simulations. Convex optimization is used to achieve beam steering and flexible and adaptive nulling. The use of transmitter beam-forming before applying DOA algorithms (which is only possible using a MIMO system) will produce an SNR improvement of $10 \log_{10} 33 = 15.185$ dB from beam-forming using 33 transmitters and 3 dB from the element pattern for a total of 18.2 dB. Transmitter beam-forming can be used to reject clutter by 20 dB (in azimuth and elevation) in the near field and up to 15 dB in the far field. Flexible nulling can reduce the magnitude of interferers still further. Using these techniques we are able to avoid the MEMP limitation on the number of targets and also reduce the interference between targets.

ACKNOWLEDGMENT

The authors acknowledge the Australian Research Council for their financial support, under Linkage Grant LP0669638, the University of New South Wales at the Australian Defense Force Academy for infrastructure support, Termatrac Pty Ltd and Scientific Technology

Pty Ltd (industrial partners) for their facilities and equipment for this project. The authors further acknowledge A. Prof Donald Fraser and Prof. Joseph Lai for helpful suggestions in preparing this manuscript and Gerard Rankin for editing and contributions to the research.

REFERENCES

1. Caulfield, R. and P. Daly, "An analysis of termite damage in Sydney and Melbourne," Hawthorn, Victoria, Australia, 2006.
2. Tirkel, A. Z., G. J. Sanderson, and R. J. Davies, "Termite detection system," 6313643, June 11, 2001.
3. "National telecommunications and information administration," Federal Standard 1037C, 1996.
4. Le Marshall, N. W. D. and A. Z. Tirkel, "Modified matrix pencil algorithm for termite detection with high resolution RADAR," *Progress In Electromagmnetics Research C*, Vol. 16, 51–67, September 2010.
5. Le Marshall, N. W. D., G. A. Rankin, and A. Z. Tirkel, "High resolution, wide coverage termite imager," *PIERS Proceedings*, 663–667, Xian, China, March 22–26, 2010.
6. Hua, Y., "Estimating two-dimensional frequencies by matrix enhancement and MEMP," *IEEE Transactions on Signal Processing*, Vol. 40, No. 9, 2267–2280, September 1992.
7. Paulraj, A., R. Roy, and T. Kailath, "Estimation of signal parameters via rotational invariance technique — ESPRIT," *IEEE Transactions on Acoustics, Speech and Signal Processing*, Vol. 37, No. 7, 984–995, July 1989.
8. Schmidt, R. O., "Multiple emitter location and signal parameter estimation," *IEEE Transactions on Antennas and Propagation*, Vol. 34, No. 3, 276, March 1986.
9. Bachl, R., "The forward-backward averaging technique applied to TLS-ESPRIT processing," *IEEE Transactions on Signal Processing*, Vol. 43, No. 11, 2691–2699, November 1995.
10. Le Marshall, N. W. D. and A. Z. Tirkel, "The application of the MEMP and beamforming to determine the presence of termites in situ," *IEEE Eurocon 2009 Proceedings*, 1568–1572, 2009.
11. Le Marshall, N. W. D., G. A. Rankin, and A. Z. Tirkel, "Hybrid array for the detection and imaging of termites," *Radio and Wireless Symposium 2010*, 288–291, New Orleans, USA, 2010.
12. Brown, G., "Spartan-DSP takes aim at affordable DSP performanc," *DSP Magazine*, No. 3, 8–9, 2007.

13. Burintramart, S. and T. Sarkar, "Target localization in three dimensions," *Advances in Direction of Arrival Estimation*, Artech House, 2005.
14. Friedlander, B., "Direction finding using an interpolated array," *International Conference on Acoustics, Speech and Signal Processing*, Vol. 5, 2951–2954, 1990.
15. Kyungjung, K., T. K. Sarkar, and M. S. Palma, "Adaptive processing using a single snapshot for a nonuniformly spaced array in the presence of mutual coupling and near-field scatterers," *IEEE Transactions on Antennas And Propagation*, Vol. 50, No. 5, 582–590, May 2002.
16. Donnet, B. J. and I. D. Longstaff, "MIMO radar, techniques and opportunities," *3rd European Radar Conference, 2006*, 112–115, Manchester, September 2006.
17. Everett, D., "Periodic digital sequences with pseudonoise properties," *GEC Journal*, Vol. 33, No. 3, 115–126, 1966.
18. Bak, P., C. Tang, and K. Wiesenfeld, "Self-organized criticality: An explanation of the $1/f$ noise," *Physical Review Letters*, Vol. 59, No. 4, 381–384, 1987.
19. Schottky, W., "Small-shot effect and flicker effect," *Physical Review*, Vol. 28, No. 6, 1331, 1926.
20. Dandekar, K. R., L. Hao, and X. Guanghan, "Experimental study of mutual coupling compensation in smart antenna applications," *IEEE Transactions on Wireless Communications*, Vol. 1, No. 3, 1536–1276, July 2002.
21. Boyd, S. and L. Vandenberghe, *Convex Optimization*, Cambridge University Press, March 2004.
22. Boyd, M. and S. Grant, "CVX: MATLAB software for disciplines convex programming," June 2009, http://stanford.edu/∼boyd/cvx.
23. Toh, K., M. J. Todd, and R. H. Tutunc, "SDPT3 — A MATLAB software for semidefinite-quadratic-linear programming, 2009, http://www.math.nus.edu.sg/∼mattohkc/sdpt3.html.
24. Lebret, H. and S. Boyd, "Antenna array pattern synthesis via convex optimization," *IEEE Transactions on Signal Processing*, Vol. 45, No. 3, 526–532, March 1997.
25. Albagory, Y. A., M. Dessouky, and H. Sharshar, "An approach for low sidelobe beamforming in uniform concentric circular arrays," *Wireless Personal Communications*, Vol. 43, No. 4, 1363–1368, June 2007.